Model Uncertainty Quantification for Column Removal Scenario Calculations Using the Energy-based Method

Luchuan DING, Wouter BOTTE, Ruben VAN COILE, Robby CASPEELE

Department of Structural Engineering and Building Materials,
Ghent University,
Technologiepark Zwijnaarde 60, Ghent (9052), Belgium

Abstract

Progressive collapse resistance of a building structure is often investigated by the notional removal of one or more vertical load bearing elements from the structural system. Usually, a nonlinear dynamic analysis is needed to perform such an analysis. To avoid the complex nonlinear dynamic analysis, the energy-based method (EBM) is a promising method to predict the maximum dynamic responses of a structural system, where the dynamic load-bearing capacity curve is derived from the static load-displacement curve based on the principle of energy conservation. In this contribution, the performance of the EBM is evaluated based on a validated finite element model of a tested RC slab. Subsequently, 60 samples are generated by using Latin Hypercube Sampling (LHS), taking into account probability distributions for the most important variables. Both static analyses and direct dynamic analyses are executed for every sample set. Based on the results of the stochastic analyses, the EBM is observed to perform well. Furthermore, in the analyzed case study, the model uncertainty of the ultimate load-bearing capacity obtained through the EBM compared to direct dynamic analysis is found to be represented well by a lognormal distribution with mean (i.e. bias) of 0.96 and a standard deviation of 0.13. Model uncertainties are also obtained in relation to ultimate displacements and displacements at different load levels.

1 Introduction

The Alternative Load Path (ALP) method is a widely used method for robustness assessments based on the notional member removal concept [1][2]. A sudden column removal scenario is usually used in the ALP method to check the capability of the structural system to develop alternative load paths to redistribute the unbalanced forces [3][4]. However, the analysis of such an event is complex since both nonlinear behaviors and dynamic effects are involved. Although a direct nonlinear dynamic analysis can provide an accurate result, it requires significant numerical expertise to perform the analysis and introduces high computational demands.

The energy-based method (EBM) is an alternative simplified approach for such kind of analysis, without the need to carry out any direct dynamic analyses. The EBM is based on the principle of conservation of energy, which makes it easy to understand and apply. This approach has been validated when applied to sudden column removal scenarios [5]-[8].

The EBM is based on several simplifications and, therefore, an approximate result is obtained which is a compromise between accuracy and complexity. Furthermore, several uncertainties exist within structural analysis which may have a significant influence on the overall behavior. Nevertheless, most of the existing studies neglect this [2][9][10] and therefore a probabilistic analysis might yield a more comprehensive evaluation of the performance of the EBM.

Firstly, the EBM is introduced in detail. Afterwards, a numerical model is built based on the experimental results of a RC slab to validate the EBM. Next, stochastic analyses are executed to evaluate the EBM in a probabilistic way and quantify the model uncertainty. Finally, concluding remarks are presented.

2 The energy-based method

Conservation of energy must be satisfied for a structural system undergoing deformations. Considering this, the energy-based method (EBM) can be easily described in physical terms [5][6]. Assuming a structural system subjected to a sudden column removal at a certain moment in time, the equilibrium for the gravity load and external loads will not be satisfied any more due to the unbalanced forces

originating from the column before the removal. Thus, the structure accelerates, deforming in order to accommodate the unbalanced loads. The released gravity potential energy during this moving process is transferred into strain energy and kinetic energy, increasing the velocity of the system until a maximum velocity is reached. Beyond this point, the upward forces resulting from the stress-strain state exceed the downward forces from the gravity loads and the external loads. The structure slows down again, while the additional absorbed strain energy leads to a reduction in the kinetic energy. Finally, the kinetic energy is reduced back to zero (i.e. the velocity is equal to zero). Neglecting the energy dissipated by other sources such as heat, the absorbed strain energy then equals the released potential energy and enables to quantify the maximum deflection.

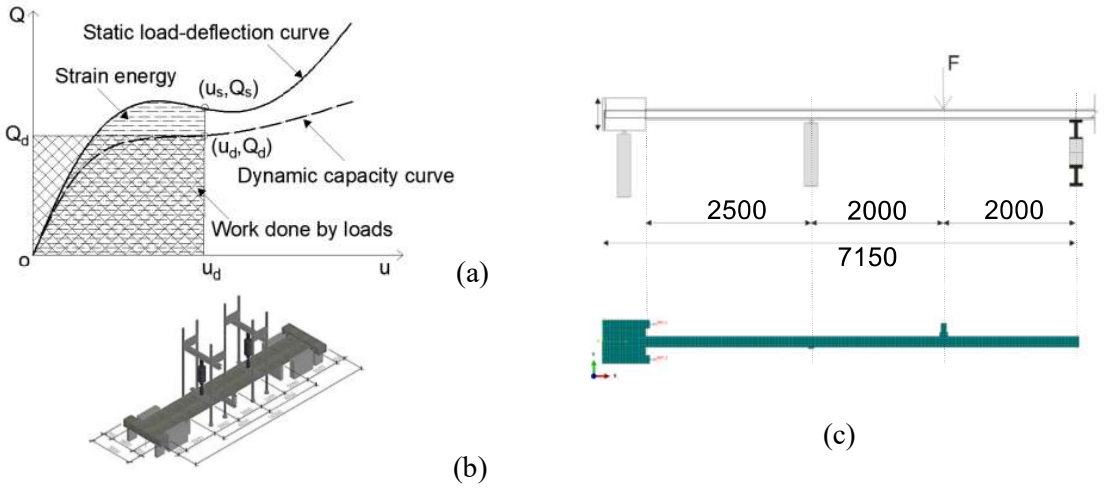

Fig. 1 Concept of the energy-based method (a) [6]; test set-up (b) [11]; detail of half of the test set-up and the corresponding FE model (c).

To apply the EBM, the strain energy is calculated first through a quasi-static nonlinear pushdown analysis. The strain energy is equal to the area under the static load-deflection curve (see Fig. 1 (a)). Considering that the released potential energy from the loads at the displacement u_d and the internal stored strain energy are equal at the same displacement level, i.e. the hatched rectangular area corresponding to (u_d, Q_d) equals the hatched area under the static load-deflection curve until (u_s, Q_s), the dynamic load Q_d can be mathematically calculated by using (1),

$$Q_d(u_d) = \frac{1}{u_d}\int_0^{u_s} Q_s(u)du \tag{1}$$

where Q_d is the load in the dynamic load-deformation curve; Q_s is the load in the static load-deformation curve; u_d is the peak dynamic deflection; and u_s is the static deflection.

3 Validation of the energy-based method

3.1 Finite element model

An experiment on a real-scale one-way slab subjected to a removal of a support [11] is employed to develop a finite element model (FEM). The test set-up is illustrated in Fig 1 (b). The total length of the slab was 14.3m with two inner spans of 4m and two outer spans of 3.15m. The width of the specimen was 1.8m. Concrete of class C30/37 was used, while the flexural reinforcement consisted of 16 bars of type S500 with a nominal diameter of 10mm for both top and bottom reinforcements. The concrete cover was 20mm. Material properties of both the concrete and the steel are summarized in Table 1. In addition, only the inward movements were restrained by heavily reinforced edge beams at two ends of the slab since the experiment aimed at investigating tensile membrane action only. Additional details can be found in the related paper [11].

The FE software Abaqus is employed to perform the numerical analysis. Considering the symmetry of both geometry and loading, a 2D plane stress FEM of half of the slab is modelled. As cracks are expected to occur all over the slab, a dense mesh is applied, i.e. 8 elements through the slab depth, see Fig. 1 (c) and 2 (d). 4-node bilinear plane stress quadrilateral elements (CPS4R) are used to model the concrete. The parabolic stress-strain relationship is implemented for concrete in compression, while the

Hordijk tension softening model is used for concrete in tension, see Fig. 2 (a) and (b) [12]. The concrete damaged plasticity (CDP) model is used. For the reinforcement, 2-node linear truss elements (T2D2) are applied assuming perfect bond to the neighboring concrete elements. A multi-linear stress-strain relationship based on laboratory testing is employed for the reinforcement, i.e. the strain hardening of steel is considered as an elastic-plastic model which explicitly includes a sudden decrease in strength at rupture of the reinforcement bars to enable to model the observed failure phenomenon of the slab, see Fig. 2 (c). The parameters from Table 1 are used.

Table 1 Material properties for concrete and reinforcing steel [11].

Concrete		Steel			
f_c (MPa)	E_{ci} (GPa)	f_y (MPa)	f_t (MPa)	ε_u (%)	E_s (GPa)
36.2	31.97	555	605	8.31	207.9

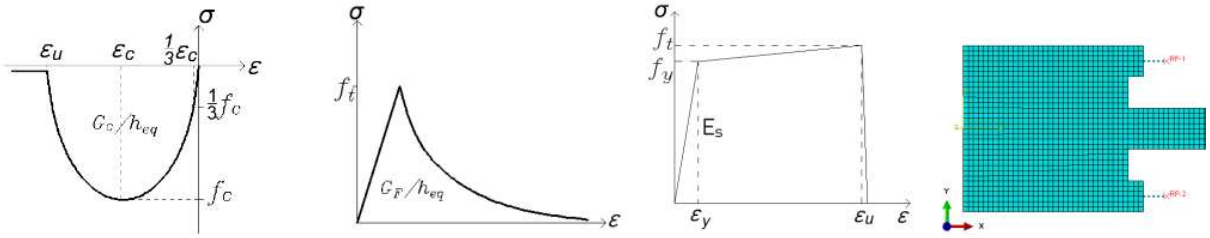

(a) (b) (c) (d)

Fig. 2 Stress-strain relationships of concrete and reinforcement [12] and springs in the FEM: concrete in compression (a); concrete in tension (b); reinforcement (c); boundary condition (d).

Lateral displacements over the central support are prohibited considering the symmetry condition. As in the experimental test set-up, the outward movement of the edge beam is allowed. However, the inward movement is restrained through spring elements, see Fig. 2 (d). Two connector elements are employed to simulate springs, incorporating the relationship between the occurring horizontal force and the corresponding horizontal displacement. Based on the measured membrane force versus displacement measurements on the end blocks in the test setup, the spring stiffness is assigned as a constant value of 151.5kN/mm for each spring.

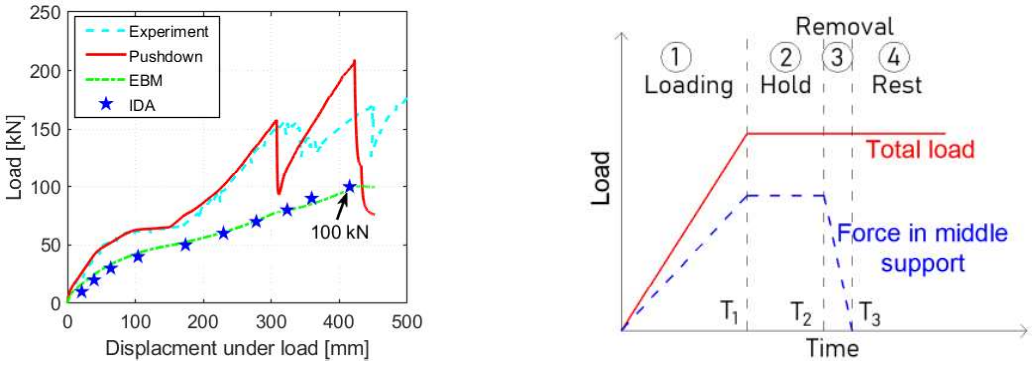

(a) (b)

Fig. 3 Vertical load-deformation relationship (a); Loading scheme for the dynamic analyses (b).

To validate the FEM, the same loading scheme as the test is executed, which is divided into three loading phases. The self-weight and a service load of 60kN are initially applied, followed by the removal of the service load in phase 1. The central support is removed in phase 2, i.e. the two inner spans of 4m thus become one span of 8m. Eventually, a displacement controlled vertical load is imposed on the slab in phase 3 until the failure of the slab. Abaqus/Standard is employed to perform the static pushdown analysis. Geometrical nonlinearities are taken into account. The load-displacement curves obtained from both the experiment and the numerical pushdown analysis are presented in Fig. 3 (a), where good agreement between both is observed until the first load peak. Similar as observed in the experiment [11], the slab experiences an elastic stage, an elastic-plastic stage and a tensile membrane

action stage. Little difference is found between the values of the first load peaks, which are 158.1kN and 156.6kN, respectively. This first load peak corresponds to rupture of the reinforcement over the inner support. The subsequent structural response is highly complex which is reflected by the significant discrepancy between experiment and numerical analysis. In case structural failure is defined as first rupture of reinforcement, it can be concluded that the FEM has a good performance.

3.2 Comparing between the EBM and direct dynamic analyses

Based on the EBM and the results presented in 3.1, a dynamic load-bearing curve is calculated and presented in Fig. 3 (a). The ultimate dynamic load-bearing capacity is 100.4kN. The sudden decrease in strength occurring on the pushdown curve is not observed on the dynamic capacity curve since the latter is calculated from the former based on the energy balance. However, a slight softening stage on the dynamic capacity curve is observed between 80kN and 100kN.

As the dynamic capacity curve is directly derived from pushdown curve without performing any dynamic analyses, the effectiveness of the EBM can be validated by comparing the derived dynamic capacity curve with results of direct dynamic analyses. The incremental dynamic analysis (IDA) technique is employed here to execute the dynamic analyses on the same FEM, which performs a series of dynamic analyses from a lower load to a higher load until the collapse of the slab occurs. A loading scheme presented in Fig. 3 (b) is used. First, self-weight and vertical loads are applied in phase 1 from 0 to T_1 (1.5s). Secondly, the loads are kept the same from T_1 to T_2 (1.5s-2.0s). Thirdly, the support is removed in a time duration of 10^{-5}s from T_2 to T_3. Thereafter, the structure keeps on oscillating with the other loads. Abaqus/Explicit is employed to execute the dynamic analyses.

The comparison of results of the incremental dynamic analyses (IDA) with that of the EBM is presented in Fig. 3 (a), in which every star represents a maximum displacement of the dynamic response under the corresponding vertical imposed load. The maximum dynamic load capacity is approximately 100kN, which agrees well with that of EBM, i.e. 100.4kN. For a higher imposed load, the structure fails in the dynamic analysis upon removal of the central support. The good agreement between EBM and IDA indicates that the EBM predicts the maximum dynamic response well. Influences of the strain rate effects and damping were investigated in another paper [7], which shows that strain rate effects are not significant and the influence of damping is limited. Therefore, these dynamic effects are not taken into account in this paper. Furthermore, it needs to be mentioned that the numerical results deviate from the observed experimental data after the first load peak was reached, but that this does not prevent to quantify the model uncertainty of the EBM compared to direct dynamic analyses as performed in the following. Nevertheless, this indicates the importance to quantify also a model uncertainty with respect to the prediction of the highly nonlinear post-peak behavior in case of large deformations and membrane actions, for which however at this stage only very limited data is available.

4 Uncertainty Quantification

4.1 *Probabilistic models for the input variables*

Based on previous investigations [2][10][13][14], eight parameters are selected as input random variables to quantify the uncertainty propagation when the EBM is used. These parameters are the material properties of concrete, the material properties of reinforcing steel, the cross-section of the reinforcement and the stiffness of the horizontal springs (see Fig. 2 (d)). The probabilistic models are presented in Table 2. The other input parameters are considered deterministic.

Table 2 Probabilistic models for the random variables.

Name	Unit	Distribution	Mean (μ)	COV
Density of concrete ρ_c	kg/m^3	N	2400	0.04
Concrete compressive strength f_c	MPa	LN	36.2	0.10
Reinforcement yield stress f_y	MPa	N	555	0.03
Reinforcement tensile strength f_t	MPa	LN	605	0.03
Reinforcement strain at maximum stress ε_u	%	LN	8.3	0.15
Young's modulus of reinforcement E_s	GPa	N	207.9	0.08

Cross-section of reinforcement A_s	mm^2	N	1256	0.02
Stiffness of horizontal spring k	kN/mm	LN	151.5	0.25

Latin Hypercube Sampling (LHS) is used in combination with the developed FEM to perform stochastic analyses, which allows to limit the number of calculations to an acceptable amount. As the standard LHS may bring undesired spurious correlation into the sample scheme, correlation Latin Hypercube Sampling (LHS) is used to avoid this unwanted effect [15]. Sixty Latin-Hypercube samples are generated based on the probabilistic models presented in Table 2. Eventually, each set of sampled realizations is used as an input for the FEM to determine the response predicted by the EBM and by IDA.

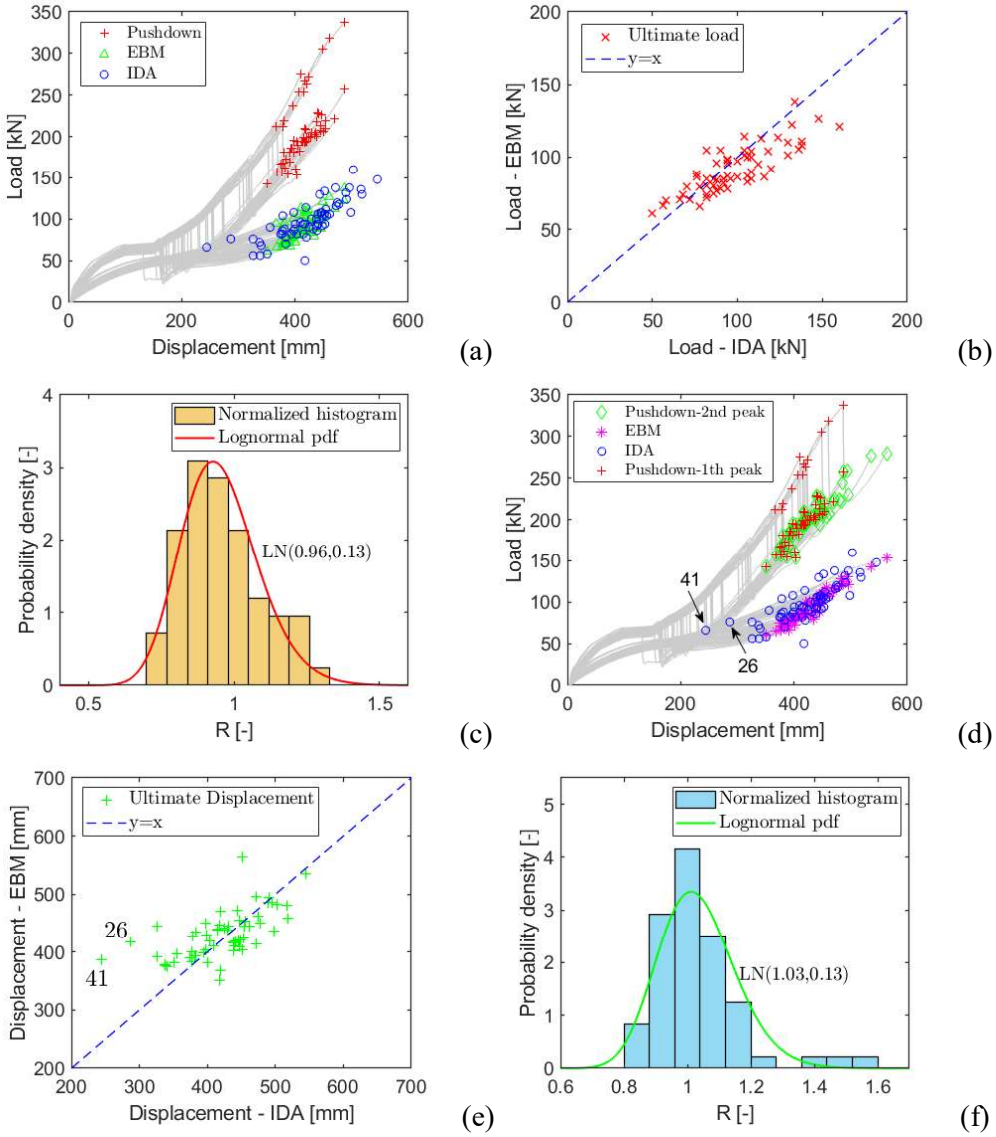

Fig. 4 Comparison for the ultimate capacities between EBM and IDA: load-displacement relationship (a); comparison of ultimate load-bearing capacity (b); histogram and PDF of the ratio (load) EBM/IDA (c); load-displacement relationship (d); comparison of displacement (e); histogram and PDF of the ratio (displacement) EBM/IDA (f).

4.2 *Stochastic analyses*

All LHS samples are evaluated considering both static pushdown analyses and direct dynamic analyses. For the latter, the IDA technique is employed for every slab realization. Firstly, a load interval of 10kN is employed from 40kN to 160kN, i.e. 13 dynamic simulations. To obtain a 2kN resolution for the maximum dynamic load, another 4 simulations are performed every 2kN in the interval between the last non-failed simulation and the first failed simulation. No smaller load interval is further considered as this requires much more calculations. Subsequently, the curves from the pushdown analyses are

converted into dynamic capacity curves (EBM) to be compared with the results of the direct dynamic analyses (IDA). The details are not presented here for every sample, however, in general, a good agreement is observed between the results of EBM and IDA.

The results of static pushdown analyses show an elastic stage, an elastic-plastic stage and a tensile membrane action stage for every realization. The dynamic capacity curves of EBM completely depend on the pushdown curves. Fig. 4 (a) present the comparisons between the EBM and IDA for ultimate load-bearing capacities. The ultimate static load-bearing capacities (pushdown) are also shown. Although differences can be observed for the corresponding displacements, the results of EBM are situated in the same load ranges as the results of IDA. Good agreement is found for the ultimate load-bearing capacities of the two cases, see Fig. 4 (b), where the ultimate load-bearing capacities of EBM against the ultimate capacities of IDA distribute along the diagonal line (y=x), i.e. the values are approximately equal to each other.

As the ultimate displacements may occur after the displacements corresponding to the ultimate load-bearing capacities in some pushdown curves, i.e. the second peak load is lower than the first peak load on the pushdown curves, see Fig. 4 (d), the dynamic capacities of EBM based on the pushdown curves will be larger in these cases. Therefore, a comparison of the corresponding ultimate displacements is also relevant. The dynamic capacities of EBM of the ultimate displacements are compared with the IDA. A good agreement is observed for the ultimate displacements of EBM against IDA as presented in Fig. 4 (e). However, two cases (26 and 41) significantly deviate.

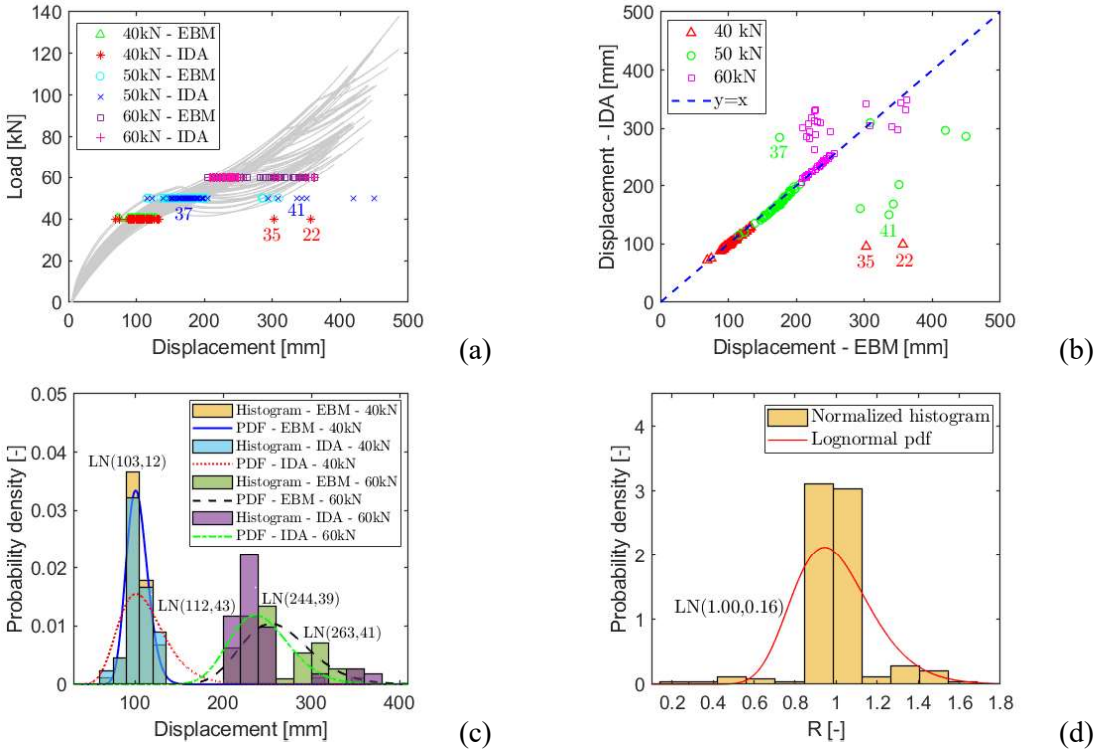

Fig. 5 Comparison of the displacements between EBM and IDA: load-displacement relationship (a); comparison of displacement (b); histograms and PDFs of the displacements (c); histogram and PDF of the ratio of the displacements corresponding to EBM/IDA (d).

The performance of the EBM for the ultimate capacities is observed to be well. The performance for other stages, i.e. the elastic-plastic stage and the tensile membrane action stage, is further assessed. As a load interval of 10kN is used in the IDA and the corresponding peak displacements are obtained, the displacements are used to compare with the EBM. Fig. 5 (a) shows the load-displacement relationships of dynamic cases under three load levels, i.e. 40kN, 50kN and 60kN, for both EBM and IDA. The displacements obtained through EBM against the displacements obtained through IDA are presented in Fig. 5 (b) for the three cases, respectively. The points distribute along the diagonal line, which indicates the displacements of EBM agree well with the displacements of IDA. However, considering a confidence level in three times of standard deviation, four cases could be considered as outliers, namely 22 and 35 in case of 40kN and 37 and 41 in case of 50kN, respectively. Further, it should be noted that only 56 samples remain available in case a load of 60kN is considered for the dynamic analysis, as the

ultimate dynamic load-bearing capacities of four cases, i.e. 22, 35, 48 and 54, are found to be smaller than 60kN. Histograms and probability density functions (PDFs) of displacements corresponding to a load of 40kN and 60kN for EBM and IDA are presented in Fig. 5 (c), respectively, where lognormal distributions are used to fit the PDFs. The PDFs for displacements are close to each other in case of 40kN, which indicates a good performance of the EBM. A larger variation is observed in case of 60kN, although the distribution for the EBM can be considered to be modeled still reasonably well. Therefore, comparing with the results of IDA, EBM can be considered overall to perform very well in both the elastic-plastic stage and in the tensile membrane action stage.

4.3 *Uncertainty quantification*

To evaluate the performance of EBM quantitatively, ratios of the displacements of the EBM to the direct dynamic analyses (IDA), see Fig. 4 (e) and 5(b), are calculated by using Eq. (2). Further, ratios of the ultimate load-bearing capacities, see Fig. 4 (b), are also calculated.

$$R = \frac{D_{EBM}}{D_{IDA}} \text{ or } \frac{P_{EBM}}{P_{IDA}} \tag{2}$$

where R is the ratio. D_{EBM} is the displacement for EBM; D_{IDA} is the peak displacements for IDA; P_{EBM} is the ultimate load-bearing capacity for EBM; P_{IDA} is the ultimate load-bearing capacity for IDA.

Histograms for the ratios of displacements are presented in Fig. 4 (f) and 5 (d). Fig. 4 (f) shows ratios of the ultimate displacements, where a lognormal distribution LN(1.03, 0.13) is used to fit the PDF. It should be noted that the two cases of significant deviation, i.e. 26 and 41, are taken into account. Fig. 5 (d) shows ratios of all the displacements under the three load levels, i.e. 40kN, 50kN, and 60kN, in which a lognormal distribution LN(1.00, 0.16) is found to represent the histogram. The four cases of large deviations are taken into account, i.e. 22 and 35 in case of 40kN, and 37 and 41 in case of 50kN, respectively. Fig. 4 (c) shows ratios of the ultimate load-bearing capacities, where a lognormal distribution LN(0.96, 0.13) is found to fit the histogram. The parameters of the model uncertainty distributions are summarized in Table 3. As the mean values are approximately equal to one, on average a good performance of the EBM is found by comparing with the IDA.

Table 3 Ratios of EBM/ IDA.

Case	R [-]	
	Mean (μ)	Standard deviation (σ)
Displacement - 40kN	0.96	0.13
Displacement - 50kN	0.94	0.15
Displacement - 60kN	1.08	0.16
Displacement - 40kN, 50kN and 60kN	1.00	0.16
Displacement - ultimate	1.03	0.13
Ultimate load-bearing capacity	0.96	0.13

5 Conclusions

The performance of the EBM is evaluated by comparing with the direct dynamic analyses. Considering a large scale test of an RC slab, a FEM is firstly validated. Next, stochastic analyses are executed considering eight stochastic input variables using Latin Hypercube sampling. The results of EBM are compared with the results of direct dynamic analyses to assess the performance of EBM in a probabilistic way.

Good performance is found for the FEM when compared with the experimental result. Furthermore, the EBM predicts the dynamic load-bearing curve well, as confirmed by dynamic load-bearing capacity evaluations.

Although there are some differences for several cases, good agreement can be found between EBM and direct dynamic analyses for the 60 realizations. On the basis of these simulations, probabilistic models have been proposed for the model uncertainty of EBM compared to direct dynamic analyses,

in particular in relation to the ultimate load-bearing capacity, the ultimate displacement and displacements at different load levels.

Acknowledgements

The authors would like to thank the China Scholarship Council for the financial support provided in relation to the PhD research of the first author.

References

[1] Adam, J. M., Parisi, F., Sagaseta, J., and Lu, X. 2018. "Research and practice on progressive collapse and robustness of building structures in the 21st century." *Engineering Structures* 173:122-149.

[2] Feng, D. C., Xie, S. C., Xu, J., and Qian, K. 2020. "Robustness quantification of reinforced concrete structures subjected to progressive collapse via the probability density evolution method." *Engineering Structures* 202:109877.

[3] DoD 2009. "UFC 4-023-03: Unified facilities criteria - design of buildings to resist progressive collapse." Department of Defense, United States.

[4] GSA 2013. "Alternate path analysis & design guidelines for progressive collapse resistance." General Services Administration, United States.

[5] Izzuddin, B., Vlassis, A., Elghazouli, A., and Nethercot, D. 2008. "Progressive collapse of multi-storey buildings due to sudden column loss—Part I: Simplified assessment framework." *Engineering structures* 30(5):1308-1318.

[6] Herraiz, B., Russell, J., and Vogel, T. 2015. "Energy-based method for sudden column failure scenarios: theoretical, numerical and experimental analysis." Proc. IABSE Symposium Report, International Association for Bridge and Structural Engineering, Helsinki, Finland, February 11-12.

[7] Ding, L. C., Botte, W., Van Coile, R., and Caspeele, R. 2020. "Evaluation of the energy-based method for dynamic analysis under a sudden column removal scenario." Proc. The fib Symposium 2020: Concrete Structures for Resilient Society, Shanghai, China, November 22-24 (Accepted).

[8] Yu, X. H., Qian, K., Lu, D. G., and Li, B. 2017. "Progressive collapse behavior of aging reinforced concrete structures considering corrosion effects." *Journal of Performance of Constructed Facilities* 31(4):04017009.

[9] Ding, L. C., Botte, W., Van Coile, R., and Caspeele, R. 2018. "Robustness - evaluation of a stochastic dynamic system and the instant equivalent extreme - value event: The PDEM - based structural reliability evaluation of a dynamic system." *Beton - und Stahlbetonbau* 113:33-37.

[10] Ding, L. C., Droogné, D., Botte, W., Van Coile, R., and Caspeele, R. 2019. "Structural Reliability Calculations Considering Concrete Tensile Membrane Action Using the Probability Density Evolution Method." Proc. 13th International Conference on applications of statistics and probability in civil engineering (ICASP13), Seoul, South Korea, May 26-30.

[11] Gouverneur, D., Caspeele, R., and Taerwe, L. 2013. "Experimental investigation of the load–displacement behaviour under catenary action in a restrained reinforced concrete slab strip." *Engineering structures* 49:1007-1016.

[12] Hendriks, M. A., de Boer, A., and Belletti, B. 2017. "Guidelines for nonlinear finite element analysis of concrete structures." Rijkswaterstaat Technisch Document (RTD), Rijkswaterstaat Centre for Infrastructure, 1016-1.

[13] Botte, W. 2017, "Quantification of structural reliability and robustness of new and existing concrete structures considering membrane action." PhD diss., Ghent University.

[14] Droogné, D., Botte, W., and Caspeele, R. 2018. "A multilevel calculation scheme for risk-based robustness quantification of reinforced concrete frames." *Engineering Structures* 160:56-70.

[15] Olsson, A., Sandberg, G., and Dahlblom, O. 2003. "On Latin hypercube sampling for structural reliability analysis." *Structural safety* 25(1):47-68.